DELPHI Collaboration

DELPHI 2001-094 CONF 522
14 June, 2001

Results on Fermion-Pair Production at LEP running in 2000

A.Behrmann[1], I.Boyko[2], P.Checchia[3], G.Della Ricca[4], I.Gouz[5], K. Hamilton[6] J.Holt[7], T.Myklebust[8], M.Nikolenko[2], A.Olchevski[2], M.Paganoni[3], D.Reid[9], P.Renton[6], H.Wahlen[1], G.R.Wilkinson[6], M.Winter[10]

Abstract

A preliminary analysis of the data collected in 2000 with the DELPHI detector at e^+e^- collision energy above 200 GeV was performed in order to extract the hadronic and leptonic cross-sections, the leptonic forward-backward asymmetries and the polarization of τ-leptons.
Various interpretations of the results including possible physics beyond the Standard Model, are presented. In particular, the data are used to investigate potential contact interactions and for Z' bosons, and for the effects of gravity in large extra dimensions.

Contributed Paper for EPS HEP 2001 (Budapest) and LP01 (Rome)

[1]Fachbereich Physik, University of Wuppertal, Wuppertal, FRG
[2]Joint Institute for Nuclear Research, Dubna, Russia
[3]INFN, Padova, Italy
[4]INFN, Trieste, Italy
[5]INFN, Milano, Italy
[6]Department of Physics, University of Oxford, Oxford,UK
[7]CERN, Geneva, Switzerland
[8]University of Oslo, Institute of Physics, Oslo, Norway
[9]NIKHEF, Postbus 41882, NL-1009 DB Amsterdam, The Netherlands
[10]Institut de Recherches Subatomiques, IN2P3-CNRS/ULP, Strasbourg, France

1 Introduction

Preliminary results are presented from the analyses of fermion-pair final states collected in 2000 with the DELPHI experiment [1] at centre-of-mass energies, $\sqrt{s}$, up to 209 GeV. Measurements of cross-sections for inclusive hadronic, electron-positron pairs, muon-pair and tau-pair final states are given, together with leptonic forward-backward asymmetries. These results complement those obtained from data collected from 1995 to 1999 at lower collision energies from 130 to 202 GeV [2, 3, 4]. Polar angle distributions of $\mu^+\mu^-$ and $\tau^+\tau^-$ events are also given, adding to the results provided in [3, 4]. The polarisation of τ-leptons is also determined, augmenting the measurements presented in [5, 6].

The measurements of the cross-sections and forward-backward asymmetries together with the results presented in [2, 3, 4] and from LEP running in the vicinity of the Z-resonance [7, 8], are used to update the searches for new physics involving contact interactions and additional neutral gauge bosons, given in [2, 3, 4]. The data are also used to search for effects of gravity in theories with extra dimensions, updating the results given in [3, 4]. For the theoretical motivation and technical details, the reader is referred to [2, 3, 4].

Results on fermion-pair production at LEP at collision energies from 130 to 202 GeV from the other LEP collaborations can be found in [9], together with limits derived from these results.

The measurements of cross-sections, forward-backward asymmetries and angular distributions are given in section 2. The interpretations of the data are presented in section 3. A summary and conclusions are provided in section 4.

2 Measurements

2.1 Failure of part of the DELPHI TPC

During the operation of the DELPHI detector in 2000 one of the 12 sectors of the central tracking chamber, the TPC [1], failed. After the 1$^{\text{st}}$ of September it was not possible to detect the tracks left by charged particles inside the broken sector. The data affected corresponds to $\sim 1/4$ of the data collected in 2000. Nevertheless, the redundancy of the tracking system of DELPHI meant that tracks passing through the sector could still be reconstructed from signals in any of the other tracking detectors. The tracks reconstruction efficiency was slightly reduced in the region covered by the broken sector, and on average the resolution on the perigee parameters of the tracks was worse than prior to the failure of the sector. To allow studies of the data taken after the 1$^{\text{st}}$ of September samples of events have been simulated dropping information from the broken sector of the TPC. The failure of the TPC had a different impact on the analyses of each of the final states.

For electron-positron final states the impact was negligible, the energy measurements in the electromagnetic calorimeters being more important. Results are given for the two periods separately.

For the muon-pair analysis, it was decided to exclude events containing any track in the broken sector of the TPC, so that the worse momentum resolution for tracks in the TPC did not adversely effect the analysis. Similarly, for the tau-pair analysis, events were rejected if the leading track of one hemisphere of the event was in the broken sector. For both these final states, a cut on the direction of tracks in the detector is a good

approximation to a cut on the direction of the fermions. Since there are two fermions per events, the cut applied reduces the efficiency of the analyses by approximately 1/6 for the data taken with the broken TPC sector.

For hadronic final states the width of the jets in the detector means that even though the direction of the produced quarks may not point towards the broken sector of the TPC, particles may still pass through the sector. The effect of this on the analysis is non-trivial to estimate. For the results presented here only data taken up to the 1st of September were used.

Further studies of the data taken after the 1st of September are in progress. The intention is to be able to use all the available data for the final analyses.

Before the failure of the TPC sector on 1st of September, there were a number of trips of this sector of the TPC, after which the MWPC could not be run with nominal operational voltages. The voltages were adjusted to maintain tracking efficiency, but information on the specific energy loss of tracks, dE/dx, was lost in this sector.

2.2 Luminosity and centre-of-mass energy

The luminosity analysis of the data collected during LEP operation in 2000 followed closely the one described in [2, 3]. The total experimental systematic uncertainty on the preliminary determination of integrated luminosity amounts to 1.00%, to be combined with a 0.25% uncertainty reflecting the precision of the theoretical calculations underlying the computation of the cross-section visible in the luminometers. The errors are to be added in quadrature to the other sources of systematics uncertainty given below.

In previous years there has either been one distinct mean collision energy or several well separated mean collision energies for the data analysed. In 2000 the luminosity has been delivered in a distribution which is approximately a continuum. Although there are some clear peaks in the distribution of luminosity as a function of mean collision energy, the points at which to divide the data into different bins are somewhat arbitrary.

Except for electron-positron final states, the data has been divided into two ranges of collision energies for analysis: from 202.5 to 205.5 GeV and above 205.5 GeV. In this paper these are referred to as being at energies of approximately 205 and 207 GeV respectively. Figure 1 shows the distribution of luminosity as a function of centre-of-mass energy. The luminosities used for the analyses of the different final states and estimates of the mean centre-of-mass energy [10] are given in Table 1. The lower luminosity given for the hadronic final states compared to the leptonic final states, is due to the fact that only data taken before 1st of September were analysed for the former.

For electron-positron final states all data taken up to the 1st of September are analysed together as one energy point, and all data taken after that date are analysed as a second energy point. The centre-of-mass energies of these two periods are 205.4 GeV and 206.5 GeV respectively. These are referred to as being at energies of approximately 205 and 207 GeV.

The centre-of-mass energies for each of the analyses were determined from preliminary online estimates of the LEP collision energy. These are accurate to 200 MeV.

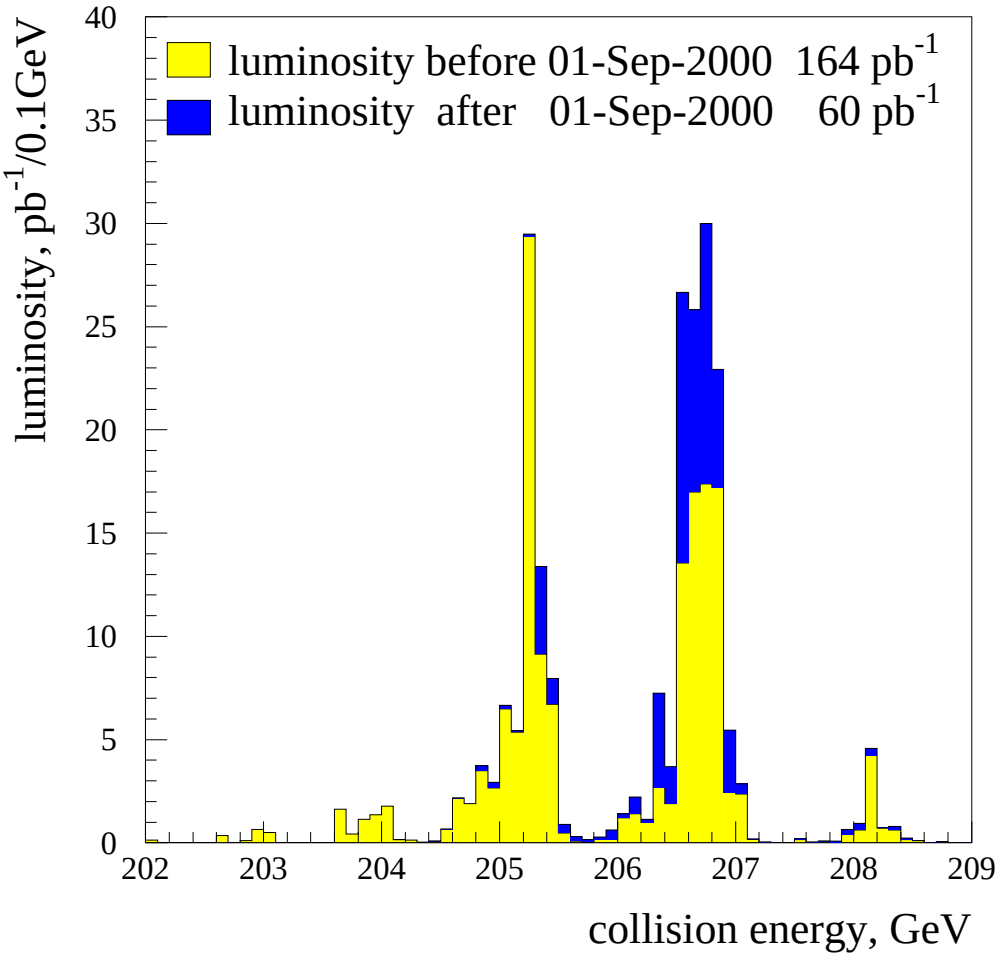

Figure 1: The distribution of luminosity as a function of energy. The luminosity is separated into that taken before and after the 1st of September. The luminosity collected in the latter period was taken with one sector of the TPC broken.

Channel	Nominal Energy (GeV)	Mean Energy (GeV)	Integrated Luminosity (pb^{-1})
$e^+e^- \to q\bar{q}(\gamma)$	205	205.0	75.0
	207	206.8	85.4
$e^+e^- \to e^+e^-(\gamma)$	205	205.4	160.0
	207	206.5	51.5
$e^+e^- \to \mu^+\mu^-(\gamma)$	205	205.0	82.5
	207	206.7	139.8
$e^+e^- \to \tau^+\tau^-(\gamma)$	205	205.1	76.3
	207	206.7	138.4

Table 1: The luminosities and collision energies for different final states. The large differences between channels are caused by the failure of part of the TPC and the different division of data into high and low energy points for the electron-positron data.

2.3 Measurements of cross-sections and asymmetries

As in [2, 3, 4], the cross-sections and asymmetry measurements are given for different ranges of the reduced centre-of-mass energy, $\sqrt{s'}$: for hadronic final states an *inclusive* sample, defined as $\sqrt{s'}/\sqrt{s} > 0.10$, and a *non-radiative* sample, defined as $\sqrt{s'}/\sqrt{s} > 0.85$; for muon and τ-lepton final states an *inclusive* sample with $\sqrt{s'} > 75$ GeV, and a *non-radiative* sample with $\sqrt{s'}/\sqrt{s} > 0.85$. For electron-positron final states, a cut on the acollinearity[1] angle between the electron and positron, $\theta_{acol} < 20^\circ$, was applied, corresponding approximately to a cut of $\sqrt{s'}/\sqrt{s} > 0.85$. The number of events selected for each final state are given in Table 2.

The results on the cross-section and leptonic forward-backward asymmetry measurements presented in this section are from the analyses of e^+e^-, $\mu^+\mu^-$, $\tau^+\tau^-$ and inclusive hadronic final states. These analyses were similar to the ones performed at lower energies and the details, such as event selection and reduced energy determination can be found, in [2, 3, 4].

The distributions of $\sqrt{s'}/\sqrt{s}$ obtained for the real and the simulated data are shown in Figure 2 for the hadronic channel and Figure 3 for the muon and τ-lepton channels. The methods of estimating $\sqrt{s'}$ correspond to slightly different definitions of this variable. For $\mu^+\mu^-$ and the $\tau^+\tau^-$ final states, $\sqrt{s'}$ is the invariant mass of the muons or τ-leptons in the final state. For the inclusive hadronic final states, the estimated $\sqrt{s'}$ can be considered in theoretical predictions to be the invariant mass of the s-channel propagator.

For the $\mu^+\mu^-$ and $\tau^+\tau^-$ final states, the cross-sections and asymmetries were extrapolated to 4π acceptance using samples of events generated with KORALZ [15]. The calculations of KORALZ do not account for interference between Initial State and Final State Radiation. Corrections to the extrapolation for this interference were determined using the semi-analytical calculations of ZFITTER [16], in which the interference was computed to $\mathcal{O}(\alpha)$, and applied to the results. To account for missing higher order corrections, a systematic uncertainty of half the correction was taken. For the inclusive hadronic states, any correction for the interference between initial and final state radiation was estimated to be negligibly small within the precision of the measurement.

Additional systematic errors were applied to the data analysed after the 1$^{\text{st}}$ of September, to account for uncertainties arising from the removal of events in the angular region covered by the broken sector of the TPC. These were 0.3% and 3% for the cross-sections in the $e^+e^-\to\mu^+\mu^-$ and $e^+e^-\to\tau^+\tau^-$ channels respectively.

For the $\mu^+\mu^-$ and $\tau^+\tau^-$ final states, the measurements from the two periods, before and after 1$^{\text{st}}$ of September, were combined. The cross-section results in the two periods were averaged together using a weighted average taking into account the correlations between the systematic errors in the two periods. The forward-backward asymmetries were combined by adding together the numbers of signal events in each period.

The measured cross-sections and forward-backward asymmetries for the different final states, and the theoretical expectations, for collisions energies above 200 GeV are given in Table 3. Figures 4 shows the measured hadron, electron-positron pair, muon-pair and τ-lepton pair cross-sections from DELPHI for all collision energies ranging from 130 up to 207 GeV. The forward-backward asymmetries for electron-positron pairs, muon-pairs and τ-lepton pairs are shown in Figure 5. The Standard Model (SM) predictions are from the

[1]The acollinearity angle between two particles is defined as $\cos\theta_{acol} = -\mathbf{p_1}.\mathbf{p_2}/|\mathbf{p_1}||\mathbf{p_2}|$, where $\mathbf{p_1}$ and $\mathbf{p_2}$ are the 3-momenta of the particles.

Channel	Collision Energy (GeV)	
	~ 205	~ 207
$e^+e^- \to q\bar{q}(\gamma)$	6292	7017
$e^+e^- \to e^+e^-(\gamma)$	2702	935
$e^+e^- \to \mu^+\mu^-(\gamma)$	393	634
$e^+e^- \to \tau^+\tau^-(\gamma)$	252	373

Table 2: The statistics used in the analyses of the different final states. For each channel, the values refer to the samples with $\sqrt{s'/s} > 0.10$ for hadrons, $\sqrt{s'} > 75$ for muons and τ-leptons and $\theta_{acol} < 20^\circ$ for electron-positron pairs.

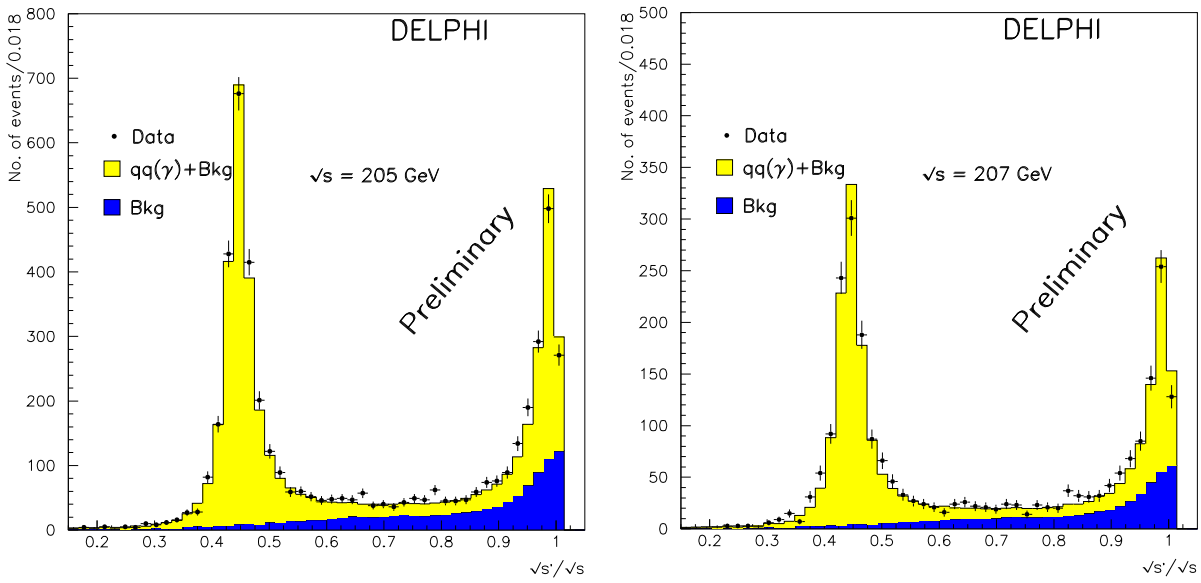

Figure 2: Distributions of the reconstructed reduced energy for the $e^+e^- \to q\bar{q}(\gamma)$ process at $\sqrt{s} \sim 205$ and 207 GeV. The points show the real data, and the histograms show the simulated signal and background samples. The expected signals are simulated with the PYTHIA [11] generator and are normalised to the luminosities of the data set analysed. Differences between data and simulation in the shape of these distributions are taken into account when determining the systematic errors on the measured cross-sections.

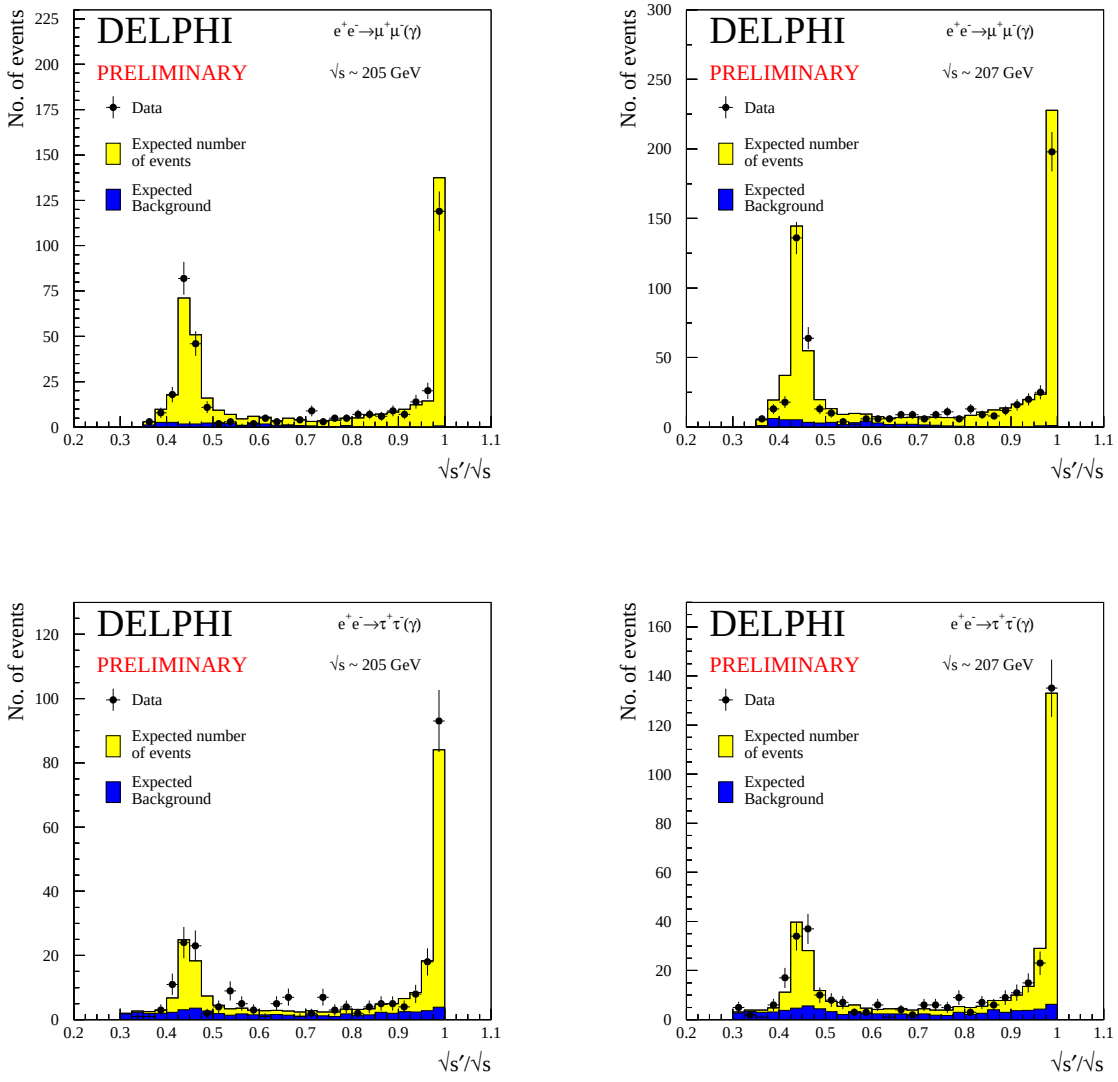

Figure 3: Distributions of the reconstructed reduced energy for the $e^+e^- \to \mu^+\mu^-(\gamma)$ and $e^+e^- \to \tau^+\tau^-(\gamma)$ processes at $\sqrt{s} \sim 205$ and 207 GeV. The points stand for the data and the histograms represent the signal and background. The expected signals are simulated with the KORALZ [15] generator scaled to the ZFITTER [16] predictions and are normalised to the luminosities of the data sets analysed.

TOPAZ0 program [17] for electron-positron final states and the ZFITTER program [16] for the others.

Statistical uncertainties and systematic errors due to the event selection and to the residual background subtraction are shown in Table 4. For the cross-section measurements, they are to be added in quadrature to the uncertainty coming from the luminosity determination. The uncertainties on the theoretical predictions for the s-channels $e^+e^-\to\mu^+\mu^-$, $e^+e^-\to\tau^+\tau^-$ and inclusive hadronic cross-sections are estimated to be below 1%.

Overall, no substantial departure of the measurements from the Standard Model predictions was found.

2.4 Measurements of differential cross-sections

In addition to the measurements of the cross-sections and asymmetries, the differential cross-sections, $d\sigma/d\cos\theta$, were measured for the $\mu^+\mu^-$ and $\tau^+\tau^-$ final states for the *non-radiative* samples.

For the $\mu^+\mu^-$ final states, the scattering angle θ is the angle of the negative fermion with respect to the incoming electron in the laboratory frame. For the $\tau^+\tau^-$ final states, the angle is defined as in [3].

Due to low statistics in the samples taken at 205 GeV after the 1$^{\rm st}$ of September in the $e^+e^-\to\tau^+\tau^-$ channel, this data was not analysed. Where present data from before and after the 1$^{\rm st}$ of September were combined by taking a weighted average of the measured differential cross-sections.

The results of the measurements of the differential cross-sections, are given in Tables 5 and 6 for $\mu^+\mu^-$ and $\tau^+\tau^-$ final states respectively. The differential cross-sections for $\sqrt{s}\sim 205$ and 207 GeV for $\mu^+\mu^-$ and $\tau^+\tau^-$ final states are shown in Figure 6. The Standard Model expectations evaluated with ZFITTER are shown for comparison.

The $\mu^+\mu^-$ final states seem to be systematically lower than the expectation, and indeed the luminosity weighted average cross-section for $e^+e^-\to\mu^+\mu^-$ is ~ 1.4 statistical standard deviations below the expectation. Averaging the deviations of the $d\sigma/d\cos\theta$ measurements from the expectations in 2000, with measurements at other energies, shows no systematic trend in the data. Overall, no substantial departure of the measurements from the Standard Model predictions was found.

2.5 Measurement of the polarisation of τ-leptons

Selected non-radiative τ-lepton pair events were used to measure the average polarisation of τ-leptons produced at energies well above the Z-resonance. One-prong hadronic τ-lepton decays, $\tau^-\to\pi^- n\pi^0$ (n ≥ 0), were selected inclusively, without separation of the different hadronic decay modes. The polarisation was extracted from distributions of angular observables which characterise the decays of τ-leptons and possible subsequent decays of hadronic resonances.

The preliminary results obtained from 1997-1999 DELPHI data were reported in [5]. The details of event selection and analysis procedure can be found there.

As discussed above, the dE/dx measurement in one sector of the TPC was unreliable throughout the year. Since this information is vital for the rejection of the electron background, the τ-lepton decay candidates found within the angular acceptance of this

Energy (GeV)		~ 205	~ 207
σ_{had} (pb)	$\sqrt{s'}/\sqrt{s} > 0.85$	17.5 ± 0.6	17.1 ± 0.5
	Theory	17.7	17.3
	$\sqrt{s'}/\sqrt{s} > 0.10$	79.1 ± 1.3	77.5 ± 1.2
	Theory	79.5	77.9
$\sigma_{\mu\mu}$ (pb)	$\sqrt{s'}/\sqrt{s} > 0.85$	2.31 ± 0.18	2.40 ± 0.18
	Theory	2.56	2.51
	$\sqrt{s} > 75$GeV	5.49 ± 0.28	5.51 ± 0.22
	Theory	5.91	5.85
$\sigma_{\tau\tau}$(pb)	$\sqrt{s'}/\sqrt{s} > 0.85$	2.70 ± 0.28	2.52 ± 0.21
	Theory	2.63	2.58
	$\sqrt{s} > 75$GeV	6.46 ± 0.51	5.90 ± 0.39
	Theory	5.95	5.83
$A_{FB}{}^{\mu}$	$\sqrt{s'}/\sqrt{s} > 0.85$	0.612 ± 0.060	0.574 ± 0.049
	Theory	0.573	0.571
	$\sqrt{s} > 75$GeV	0.296 ± 0.048	0.363 ± 0.037
	Theory	0.311	0.311
$A_{FB}{}^{\tau}$	$\sqrt{s'}/\sqrt{s} > 0.85$	0.625 ± 0.081	0.639 ± 0.066
	Theory	0.572	0.571
	$\sqrt{s} > 75$GeV	0.396 ± 0.078	0.345 ± 0.066
	Theory	0.315	0.316
σ_{ee} (pb)	$\theta_{acol} < 20^{\circ}$	18.60 ± 0.44	20.00 ± 0.64
	Theory	19.40	19.40
$A_{FB}{}^{e}$	$\theta_{acol} < 20^{\circ}$	0.804 ± 0.011	0.816 ± 0.019
	Theory	0.820	0.820

Table 3: Results of the cross-section and asymmetry measurements for the different final states. The errors indicated are statistical only. Systematic errors related to the event selection and residual backgrounds are provided in Table 4. Those coming from the luminosity determination are given in the text. The theoretical prediction is also indicated. The hadronic, muon and τ-lepton results are corrected for all cuts, apart from the $\sqrt{s'}$ cut.

Non-radiative								
$\sqrt{s}$		$\Delta\sigma^h/\sigma^h$	$\Delta\sigma^e/\sigma^e$	$\Delta\sigma^\mu/\sigma^\mu$	$\Delta\sigma^\tau/\sigma^\tau$	$\Delta A_{FB}{}^e$	$\Delta A_{FB}{}^\mu$	$\Delta A_{FB}{}^\tau$
GeV		%	%	%	%	10^{-3}	10^{-3}	10^{-3}
~ 205	(stat.)	3.3	2.4	7.8	10.4	11	60	81
	(syst.)	2.6	1.0	3.3	3.3	$^{+10}_{-3}$	1	15
~ 207	(stat.)	3.2	3.2	7.4	8.3	19	49	66
	(syst.)	2.6	0.9	3.1	3.6	$^{+10}_{-3}$	1	15

Inclusive								
$\sqrt{s}$		$\Delta\sigma^h/\sigma^h$	$\Delta\sigma^e/\sigma^e$	$\Delta\sigma^\mu/\sigma^\mu$	$\Delta\sigma^\tau/\sigma^\tau$	$\Delta A_{FB}{}^e$	$\Delta A_{FB}{}^\mu$	$\Delta A_{FB}{}^\tau$
GeV		%	%	%	%	10^{-3}	10^{-3}	10^{-3}
~ 205	(stat.)	1.6	–	5.1	7.9	–	48	78
	(syst.)	1.8	–	3.4	4.2	–	2	15
~ 207	(stat.)	1.5	–	4.0	6.6	–	37	66
	(syst.)	1.9	–	3.6	4.2	–	2	15

Table 4: Statistical and systematic uncertainties of the *non-radiative* and *inclusive* cross section and forward-backward asymmetry measurements for the different final states. *Non-radiative* refers to $\sqrt{s'}/\sqrt{s} > 0.85$ for muon, τ-lepton and hadronic final states, and $\theta_{acol} < 20^\circ$ for electron-positron pairs. *Inclusive* refers to $\sqrt{s'}/\sqrt{s} > 0.10$ for the hadronic final states and to $\sqrt{s'} > 75$ GeV for the muon and τ-lepton final states. The luminosity uncertainties (1.00% experimental and 0.25% theoretical) are not included.

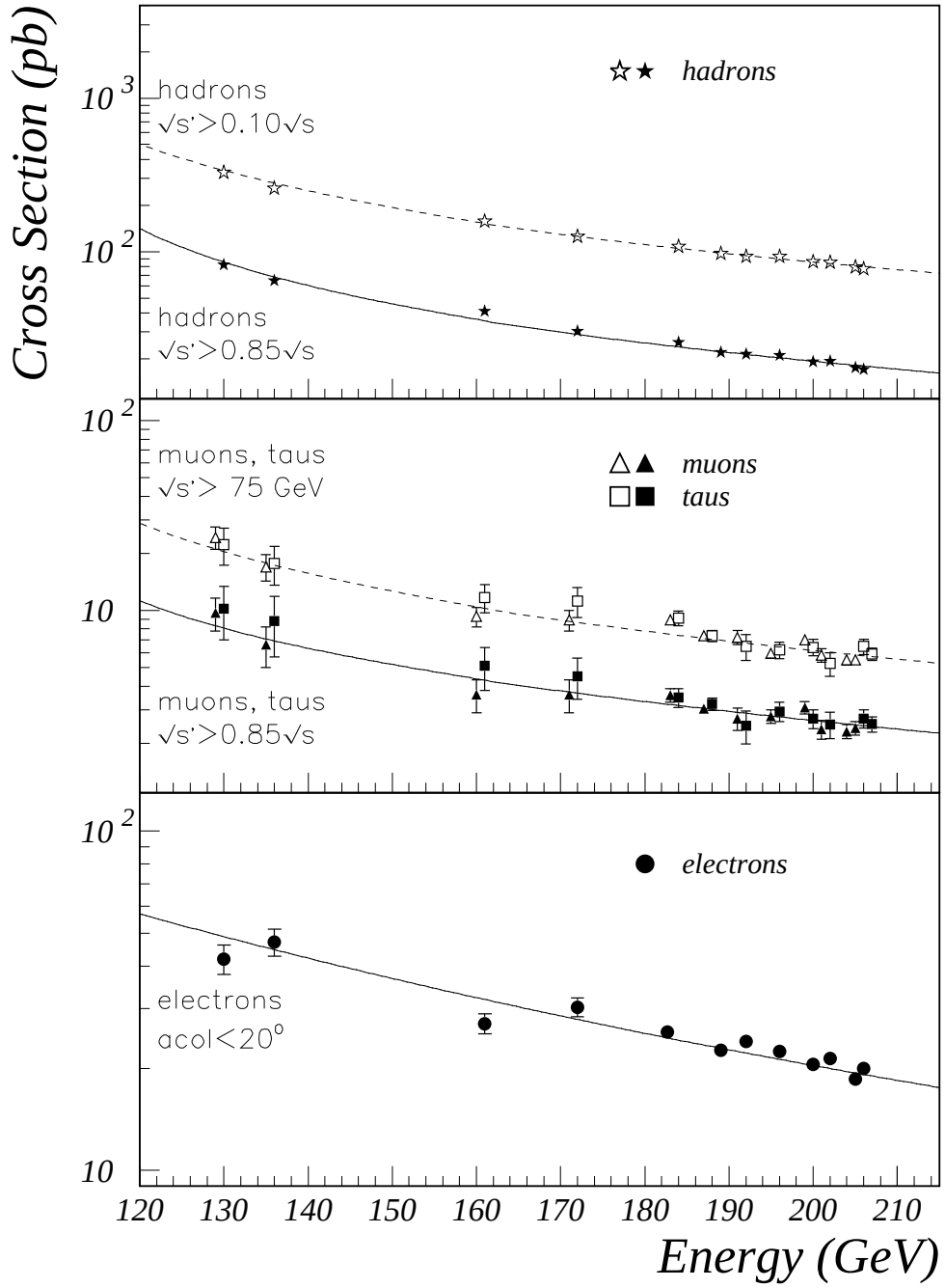

Figure 4: cross-sections for the $e^+e^- \to q\bar{q}(\gamma)$, $\mu^+\mu^-(\gamma)$ and $\tau^+\tau^-(\gamma)$, and $e^+e^- \to e^+e^-(\gamma)$ processes measured at energies from 130 up to 207 GeV. The curves show the SM prediction of the TOPAZ0 program [17] for electron-positron final states and the ZFITTER program [16] for the other final states. Open points represent the *inclusive* selections and solid points the *non-radiative* selections.

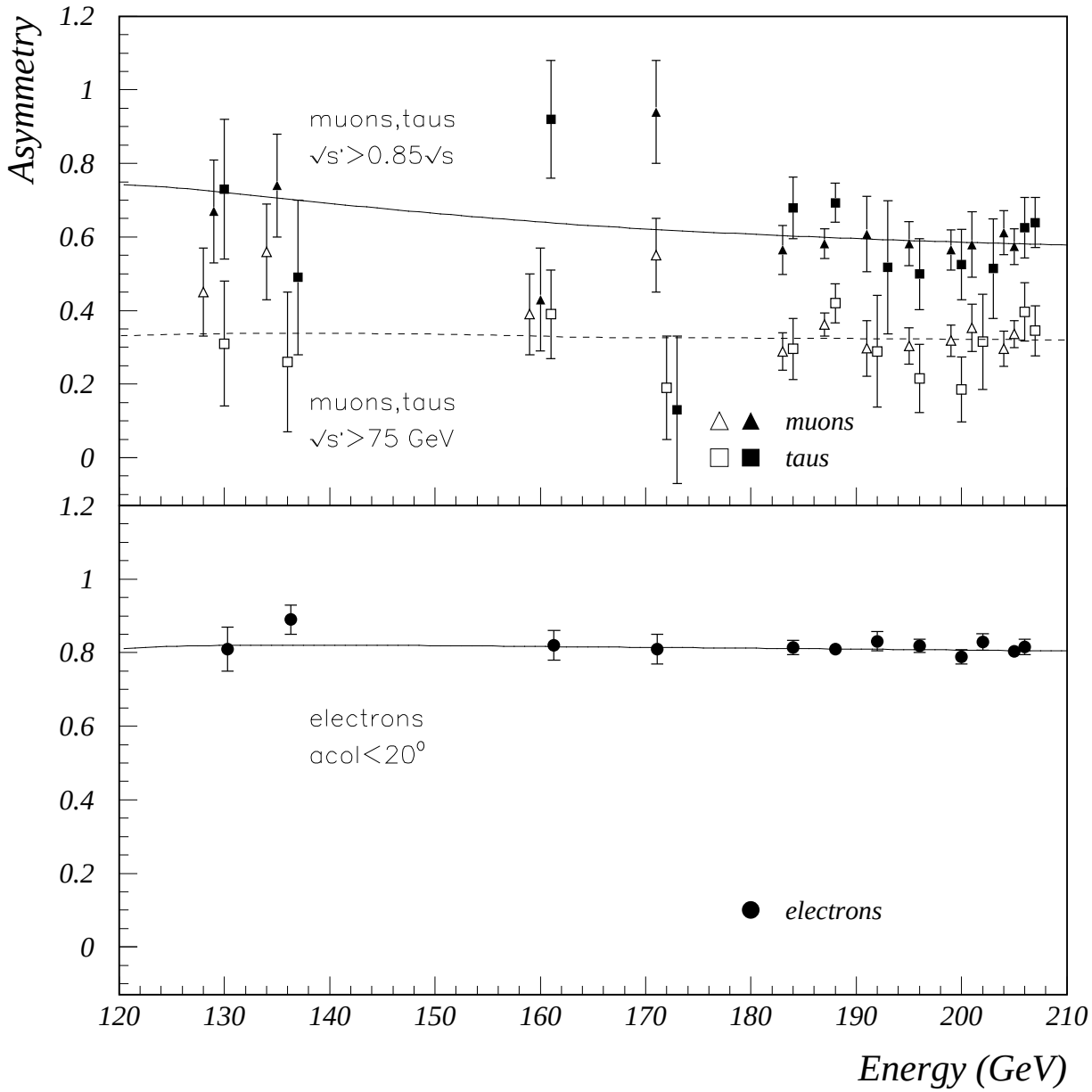

Figure 5: The forward-backward charge asymmetries in the reactions $e^+e^- \to \mu^+\mu^-(\gamma)$ and $\tau^+\tau^-(\gamma)$, and $e^+e^-(\gamma)$ measured at energies ranging from 130 to 207 GeV. The curves show the SM prediction of the TOPAZ0 program [17] for electron-positron final states and the ZFITTER program [16] for the other final states. Open points represent the *inclusive* selections and solid points the *non-radiative* selections.

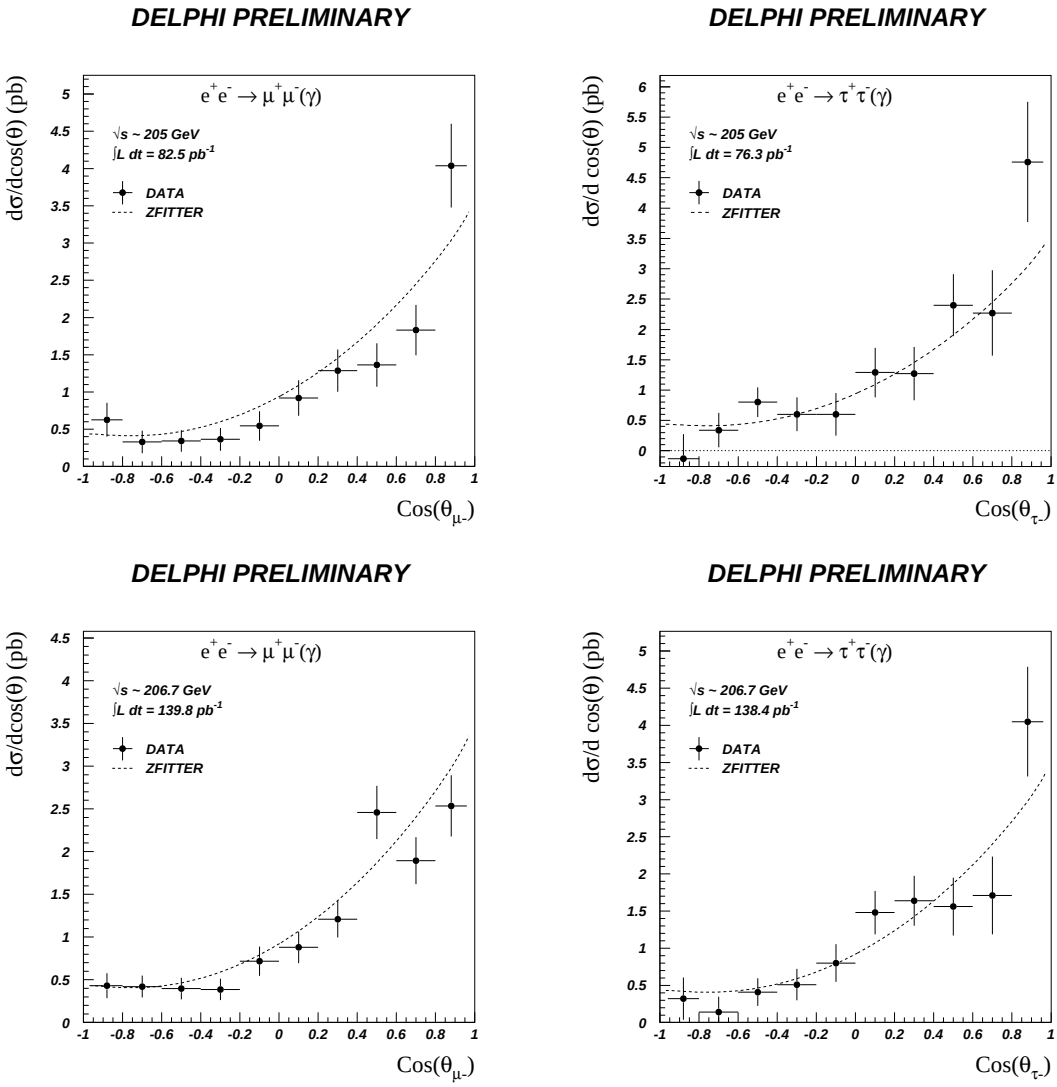

Figure 6: The weighted average of the differential cross-sections for measurements at $\sqrt{s} \sim 205-207\,\mathrm{GeV}$ for $\mu^+\mu^-$ and $\tau^+\tau^-$ final states. Also shown are the SM expectations calculated from ZFITTER for the differential cross-sections at the average value of $\sqrt{s}$.

$e^+e^- \to \mu^+\mu^-$ ($\sqrt{s} \sim 205$ GeV)		
	$d\sigma/d\cos\theta$ (pb)	
$\cos\theta$	Theory	Measurement
[-0.97,-0.80]	0.429	0.628±0.225±0.019
[-0.80,-0.60]	0.414	0.330±0.152±0.011
[-0.60,-0.40]	0.467	0.343±0.146±0.007
[-0.40,-0.20]	0.593	0.365±0.153±0.007
[-0.20, 0.00]	0.795	0.545±0.197±0.010
[0.00, 0.20]	1.075	0.919±0.237±0.016
[0.20, 0.40]	1.436	1.287±0.282±0.016
[0.40, 0.60]	1.883	1.363±0.292±0.015
[0.60, 0.80]	2.422	1.830±0.337±0.026
[0.80, 0.97]	3.076	4.039±0.561±0.040

$e^+e^- \to \mu^+\mu^-$ ($\sqrt{s} \sim 207$ GeV)		
	$d\sigma/d\cos\theta$ (pb)	
$\cos\theta$	Theory	Measurement
[-0.97,-0.80]	0.424	0.430±0.146±0.011
[-0.80,-0.60]	0.409	0.421±0.128±0.013
[-0.60,-0.40]	0.460	0.396±0.126±0.009
[-0.40,-0.20]	0.582	0.387±0.125±0.008
[-0.20, 0.00]	0.779	0.717±0.171±0.014
[0.00, 0.20]	1.054	0.879±0.183±0.016
[0.20, 0.40]	1.407	1.209±0.214±0.015
[0.40, 0.60]	1.845	2.457±0.310±0.032
[0.60, 0.80]	2.374	1.893±0.274±0.025
[0.80, 0.97]	3.016	2.535±0.357±0.029

Table 5: The differential cross-sections for $\mu^+\mu^-$ and final states at centre-of-mass energies from ~ 205 to 207 GeV. The errors shown are respectively the statistical and systematic components. The Standard Model expectations (SM) were computed with the ZFITTER program [16].

$e^+e^- \to \tau^+\tau^-$ ($\sqrt{s} \sim$ 205 GeV)		
	$d\sigma/d\cos\theta$ (pb)	
$\cos\theta$	Theory	Measurement
[-0.96,-0.80]	0.440	-0.130±0.400±0.050
[-0.80,-0.60]	0.430	0.340±0.280±0.050
[-0.60,-0.40]	0.490	0.800±0.240±0.050
[-0.40,-0.20]	0.620	0.600±0.270±0.070
[-0.20, 0.00]	0.830	0.600±0.340±0.090
[0.00, 0.20]	1.130	1.290±0.390±0.120
[0.20, 0.40]	1.500	1.270±0.410±0.160
[0.40, 0.60]	1.960	2.400±0.470±0.200
[0.60, 0.80]	2.520	2.270±0.650±0.270
[0.80, 0.96]	3.130	4.760±0.940±0.310

$e^+e^- \to \tau^+\tau^-$ ($\sqrt{s} \sim$ 207 GeV)		
	$d\sigma/d\cos\theta$ (pb)	
$\cos\theta$	Theory	Measurement
[-0.96,-0.80]	0.430	0.320±0.280±0.050
[-0.80,-0.60]	0.430	0.140±0.200±0.050
[-0.60,-0.40]	0.480	0.410±0.180±0.050
[-0.40,-0.20]	0.610	0.510±0.200±0.070
[-0.20, 0.00]	0.820	0.800±0.240±0.080
[0.00, 0.20]	1.100	1.480±0.270±0.110
[0.20, 0.40]	1.470	1.640±0.300±0.150
[0.40, 0.60]	1.930	1.560±0.340±0.190
[0.60, 0.80]	2.470	1.710±0.460±0.250
[0.80, 0.96]	3.070	4.050±0.680±0.290

Table 6: The differential cross-sections for $\tau^+\tau^-$ and final states at centre-of-mass energies from $\sim$ 205 to 207 GeV. The errors shown are respectively the statistical and systematic components. The Standard Model expectations (SM) were computed with the ZFITTER program [16].

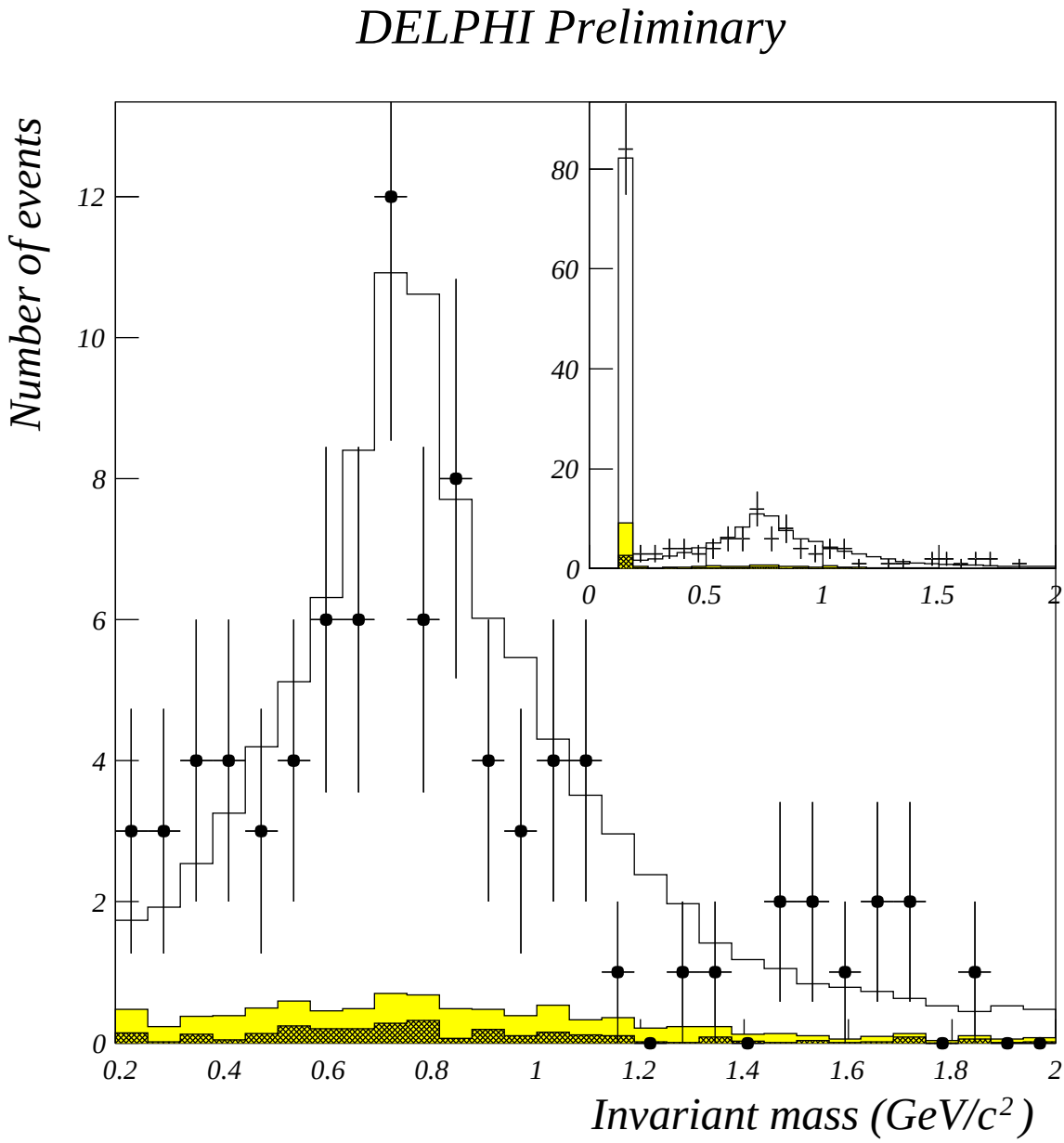

Figure 7: The invariant mass of the decay products of selected τ-lepton decays. The grey shaded region shows the expected *internal* background and the hatched shaded region shows the expected *external* background.

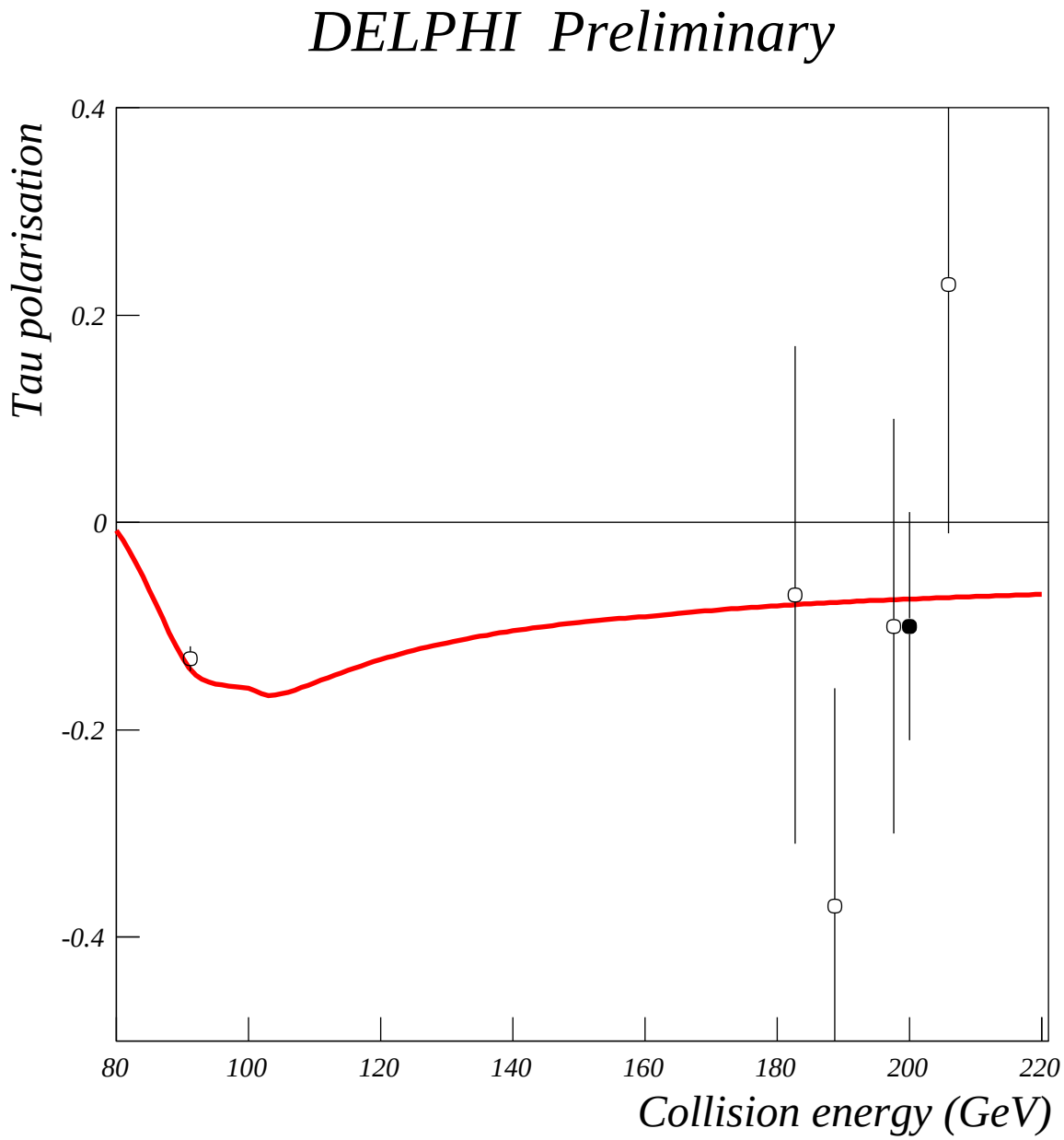

Figure 8: The τ-lepton polarisation as a function of centre-of-mass energy. The open circles are the measurements from individual years data taking. The solid point shows the averaged LEP2 result at the luminosity weighted centre-of-mass energy. Points from 183-199 GeV are taken from [5]. The point at $\sqrt{s} \sim \mathrm{M_Z}$ is from [6]. The curve shows the Standard Model prediction of ZFITTER.

sector were not considered. This reduced the data sample by about 1/12. About 170 hadronic decay candidates were selected from 2000 data (compared to approximately 630 from the data of 1997-2000). The hadronic decay selection efficiency in 2000 was 77% (within the geometrical acceptance). The residual background level was 3.2% from non-τ-lepton pair events (*external*) and 7.1% from misidentified τ-lepton decays (*internal*). The distribution of the visible invariant mass of τ-lepton decay products (charged and neutral pions) is shown in Figure 7 for decays selected from 2000 data.

The data of 2000 were analysed without separation into different LEP energies. The average LEP energy corresponding to the selected data sample was 205.90 GeV.

The fit (procedure described in [5]) has given the following value of average polarisation in 2000 data:

$$P_\tau = +0.23 \pm 0.24(\text{stat.}) \pm 0.08(\text{syst.})$$

The systematic error on the extracted polarisation, ± 0.08, is dominated by the statistics of real data samples used for calibration.

Combination of this new measurement with the preliminary DELPHI results from 1997-1999 [5] gives (at the average LEP energy of 199.4 GeV):

$$P_\tau = -0.10 \pm 0.11(\text{stat.}) \pm 0.05(\text{syst.})$$

in agreement with the Standard Model Prediction of ZFITTER:

$$P_\tau = -0.08$$

The results are shown in figure 8 together with those from [5] and [6].

3 Fits to physics beyond the Standard Model

The data presented in this paper were used to improve the constraints on physics beyond the Standard Model given in [2, 3, 4] for three sets of models. The data were used to extend the searches for contact interactions between leptons and additional neutral gauge bosons, Z′. The theoretical bases of each of these models are discussed in section 5 of [2], the key points are summarised below. Limits for models which include gravity in extra dimensions were derived from the measurements of the differential cross-sections, updating the results presented in [3, 4]. Unless otherwise stated, systematic errors for LEP2 measurements were added in quadrature with the statistical errors and treated as uncorrelated between measurements.

3.1 Contact interaction models

The parameter fitted was $\epsilon = 1/\Lambda^2$, where Λ is the scale of the interactions in the effective Lagrangian of the four-fermion interactions:

$$\mathcal{L}_{eff} = \frac{g^2}{(1+\delta)\Lambda^2} \sum_{i,j=L,R} \eta_{ij} \overline{e}_i \gamma_\mu e_i \overline{f}_j \gamma^\mu f_j, \tag{1}$$

where the i, j denote either left or right handed helicities of the fermionic currents involved. Different choices of η_{ij} lead to 12 commonly studied models, referred to as LL, RR, etc [18]. See sections 5.1 and 6.1.1 of [2] for more details.

A fit for contact interactions between leptons ($e^+e^- \to l^+l^-$), assuming lepton universality in the couplings, was made using data from $e^+e^- \to e^+e^-, e^+e^- \to \mu^+\mu^-$ and $e^+e^- \to \tau^+\tau^-$ at all energies from 130 to 207 GeV. The values of ϵ extracted for each model were all compatible with the Standard Model expectation, $\epsilon = 0$, at the two standard deviation level. The errors on ϵ are typically 10% smaller than those reported in [4] as a result of the inclusion of the new data. The fitted values of ϵ were converted into lower limits on Λ at 95% confidence level, as in [2]. The results are given in Table 7 and shown graphically in Figure 9.

3.2 Z′-bosons

Existing data from LEP1 and LEP2 and the cross-sections and asymmetries given here were used to fit the data to models including additional neutral gauge bosons, Z'.

3.2.1 Model dependent fits

Fits were made to the mass of a Z', $\mathrm{M_{Z'}}$, the mass of the Z, $\mathrm{M_Z}$, and to the mixing angle between the two bosonic fields, $\Theta_{\mathrm{ZZ'}}$, for 4 different models referred to as χ, ψ, η and L-R [19]. More details can be found in section 5.4.1 and 6.3.1 of [2]. The fitted value of $\mathrm{M_Z}$ was found to be in agreement with the value found from fits to the data with no Z'. No evidence was found for the existence of a Z'-boson in any of the models. The 95 % confidence level limits on $\mathrm{M_{Z'}}$ and $\Theta_{\mathrm{ZZ'}}$ were computed for the different models by determining the contours of the domain in the $\mathrm{M_{Z'}}-\Theta_{\mathrm{ZZ'}}$ plane where $\chi^2 < \chi^2_{min}+5.99$ [20]. The allowed regions for $\mathrm{M_{Z'}}$ and $\Theta_{\mathrm{ZZ'}}$ are shown in Figure 10. The lower limits, shown in Table 8, on the Z' mass range from approximately 336 to 503 GeV/c^2. The limits change by between 3 and 37 GeV/c^2 compared to the limits presented in [4], depending on the model.

For the Sequential Standard Model [22], which proposes the existence of a Z' with exactly the same coupling to fermions as the standard Z, a limit of $\mathrm{M_{Z'}} > 656\,\mathrm{GeV}/c^2$ is found at 95% confidence. The change is -44 GeV/c^2 on the limit given in [4].

3.2.2 Model independent fits

Fits were performed to the leptonic cross-sections and forward-backward asymmetries, for the leptonic couplings of a Z', $a^N_{l'}$ and $v^N_{l'}$, normalised for the overall coupling scale and the mass of the Z' [21]. See section 5.4.2 and 6.3.2 of [2] for more details.

Several values of the mass of the Z' were considered (i.e. 300, 500 and 1000 GeV/c^2), and the ZZ'-mixing was neglected. The limits on the normalised couplings are $|a^N_{l'}| < 0.19$ and $|v^N_{l'}| < 0.21$, a change of 0.00 and -0.03, respectively, on limits given in [4].

3.3 Gravity in Extra Dimensions

Limits on the energy scale $\mathrm{M_s}$ of models of gravity in extra dimensions have been obtained for two cases, $\lambda = \pm 1$, either constructive or destructive interference between the gravitational process and the Standard Model process [23]. For further details refer to section 3.4 of [3].

Fits to the differential cross-sections, $d\sigma/d\cos\theta$, for the parameter $\epsilon = \lambda/\mathrm{M_s^4}$ were performed using data from $\sqrt{s} \sim 205 - 207$ GeV, and also including those reported in

$e^+e^- \to l^+l^-$			
Model	ϵ (TeV^{-2})	Λ^- (TeV)	Λ^+ (TeV)
LL	$-0.0061^{+0.0059}_{-0.0054}$	8.2	10.4
RR	$-0.0058^{+0.0058}_{-0.0065}$	7.8	9.9
VV	$-0.0050^{+0.0035}_{-0.0003}$	13.4	17.8
AA	$0.0013^{+0.0045}_{-0.0016}$	14.2	10.8
RL	$-0.0112^{+0.0045}_{-0.0079}$	6.4	9.9
LR	$-0.0112^{+0.0045}_{-0.0079}$	6.4	9.9

Table 7: Fitted values of ϵ and 95% confidence lower limits on the scale, Λ, of contact interactions in the models discussed in the text for $e^+e^- \to l^+l^-$, a combination of $e^+e^- \to e^+e^-$, $e^+e^- \to \mu^+\mu^-$ and $e^+e^- \to \tau^+\tau^-$ final states in which lepton universality is assumed for the contact interactions.

Model	χ	ψ	η	L-R
$M_{Z'}^{limit}$ (GeV/c^2)	503	336	353	412
$\mid \Theta_{ZZ'}^{limit} \mid$ (mrad)	1.5	2.0	2.1	1.7

Table 8: 95% confidence level lower limits on the Z$'$ mass and upper limits on the ZZ$'$ mixing angle within the χ, ψ, η and L-R models.

Final State	$\sqrt{s}$ (GeV)	ϵ_{Best} (TeV^{-4})	λ	M_S(TeV)
$\mu^+\mu^-$	$205-207$	$-0.69^{+2.35}_{-2.66}$	-1	0.667
			$+1$	0.702
	$183-207$	$-0.23^{+1.62}_{-1.73}$	-1	0.755
			$+1$	0.777
$\tau^+\tau^-$	$205-207$	$-5.80^{+4.88}_{-4.99}$	-1	0.517
			$+1$	0.593
	$183-207$	$-2.37^{+2.79}_{-2.89}$	-1	0.612
			$+1$	0.681
l^+l^-	$205-207$	$-1.86^{+2.16}_{-2.29}$	-1	0.650
			$+1$	0.723
	$183-207$	$-0.91^{+1.50}_{-1.39}$	-1	0.749
			$+1$	0.806

Table 9: 95% confidence level lower limits on M_s in models of gravity in extra dimensions for $\mu^+\mu^-$ and $\tau^+\tau^-$ final states, and for l^+l^-, a combination of both muon and τ-lepton final states.

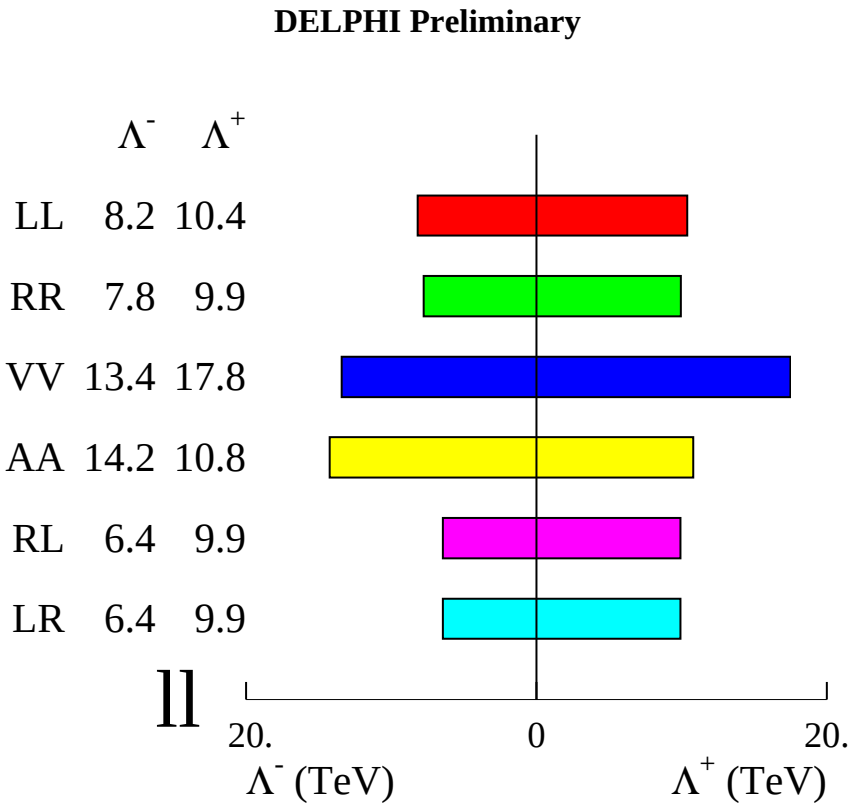

Figure 9: The limits and exclusion regions of Λ for $e^+e^- \to l^+l^-$ assuming universality in the contact interactions between $e^+e^- \to e^+e^-$, $e^+e^- \to \mu^+\mu^-$ and $e^+e^- \to \tau^+\tau^-$.

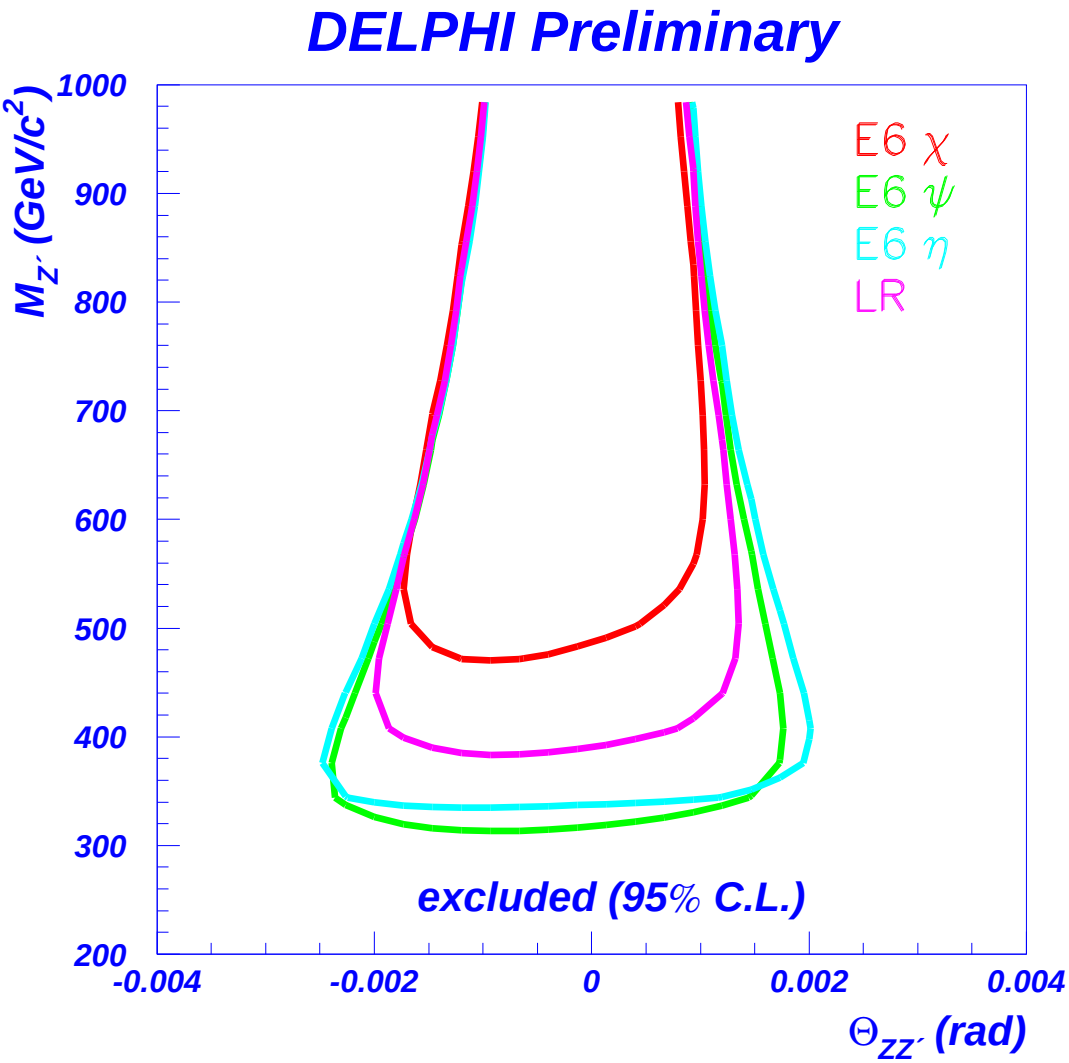

Figure 10: The allowed domain in the $M_{Z'} - \Theta_{ZZ'}$ plane for the χ, ψ, η and L-R models. The contours show the 95% confidence level limits.

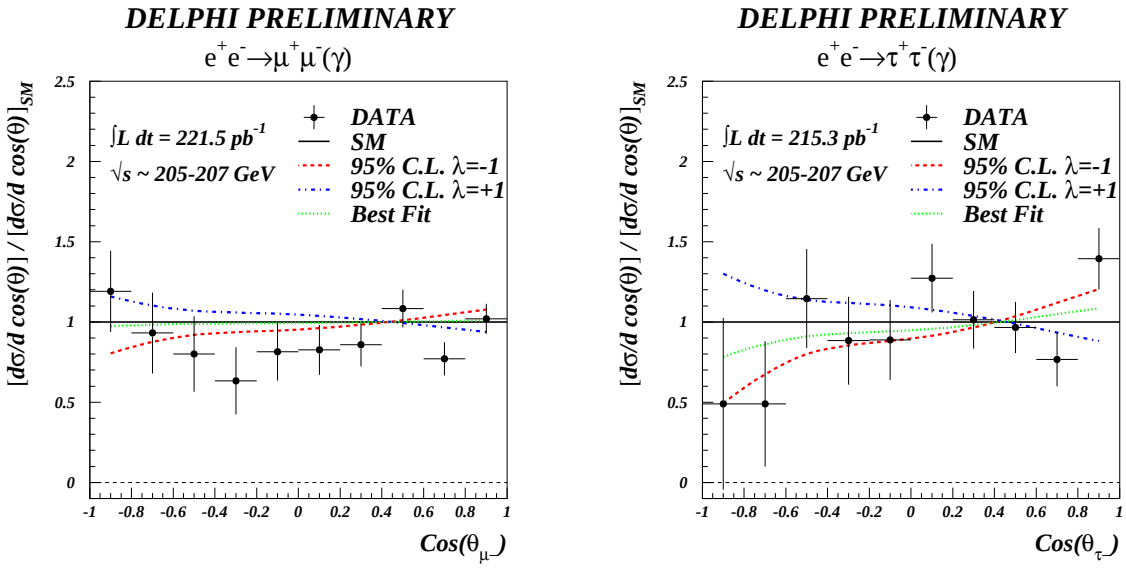

Figure 11: The weighted average of the deviations from the Standard Model angular distributions for measurements at $\sqrt{s} \sim 205 - 207$ GeV for $\mu^+\mu^-$ and $\tau^+\tau^-$ final states. Superimposed are the deviations expected from the effects of gravity in extra dimensions calculated at the combined limits for both channels and all energies for $\lambda = \pm 1$, and evaluated at the mean centre of mass energy of the data.

[3, 4]. Systematic errors correlated between bins for a given channel at a single energy where correctly handled in the fit. The fits gave values compatible with the Standard Model, i.e. $\epsilon = 0$. Table 9 shows the fitted values of ϵ and the 95% confidence level lower limits on M_s. These limits were obtained using a method equivalent to that used to extract the limits on the scale, Λ, of contact interactions, as described in section 6.1.1 of [2]. The deviations in the differential cross-sections for models of gravity in extra dimensions are compared to the data in Figure 11.

4 Summary and conclusions

The results of the preliminary determinations of cross-sections and asymmetries and differential cross-sections above 200 GeV in the channels $e^+e^- \to e^+e^-(\gamma)$, $e^+e^- \to \mu^+\mu^-(\gamma)$, $e^+e^- \to \tau^+\tau^-(\gamma)$ and inclusive $e^+e^- \to q\bar{q}(\gamma)$, have been presented.

Overall, the data agree with the Standard Model predictions of ZFITTER and TOPAZ0. The data were used to update the searches for physics beyond the Standard Model given in [2, 3, 4] and to investigate the possible effects of gravity in extra dimensions given in [3, 4]. No evidence for physics beyond the Standard Model was found, and limits were set on parameters of several more general models. The scale Λ characterising contact interactions between all leptons can be excluded at 95% confidence level in the range $\Lambda < 6.4 - 17.8$ TeV, depending on the model. Alternatively, Z' bosons lighter than $\sim 330\ \mathrm{GeV}/c^2$ can be excluded at the 95% confidence level in the models considered. Lastly, 95% confidence level lower limits of 749 and 806 GeV on the string scale, M_s, for $\lambda = -1$ and $\lambda = +1$ respectively, in models of gravity involving extra dimensions are obtained for a combinations of $\mu^+\mu^-$ and $\tau^+\tau^-$ final states.

Acknowledgements

We thank the SL Division of CERN for the excellent performance of the LEP collider and our funding agencies.

References

[1] DELPHI Collaboration, P. Aarnio *et al.* , Nucl. Instr. & Meth. **A303** (1991) 233;
DELPHI Collaboration, P. Abreu *et al.* , Nucl. Instr. & Meth. **A378** (1996) 57.

[2] DELPHI Collaboration, P. Abreu *et al.* , Eur.Phys.J. **C11** (1999) 383.

[3] DELPHI Collaboration, P. Abreu *et al.* , Phys.Lett. **B485** (2000) 45.

[4] DELPHI Collaboration, Contributed Paper 647 to ICHEP (Osaka, July 2000), DELPHI 2000-128 CONF 427.

[5] DELPHI Collaboration, I. Boyko, DELPHI 2001-021 CONF 463 (2001).

[6] DELPHI Collaboration, P. Abreu *et al.* , Zeit. Phys. **C67** (1995) 183;
DELPHI Collaboration, P. Abreu *et al.* , Eur. Phys. J. **C14** (2000) 585.

[7] DELPHI Collaboration, P. Abreu *et al.* , Nucl. Phys. **B417** (1994) 3.

[8] DELPHI Collaboration, P. Abreu *et al.* , Nucl. Phys. **B418** (1994) 403;
DELPHI Collaboration, P. Abreu *et al.* , Eur. Phys. J. **C16** (2000) 371.

[9] ALEPH Collaboration, D. Buskulic *et al.* , Phys. Lett. **B378** (1996) 373;
ALEPH Collaboration, R. Barate *et al.* , Phys. Lett. **B399** (1997) 329;
ALEPH Collaboration, R. Barate *et al.* , Euro. Phys. J. **C12** (2000) 183;
L3 Collaboration, M. Acciarri *et al.* , Phys. Lett. **B370** (1996) 195;
L3 Collaboration, M. Acciarri *et al.* , Phys. Lett. **B407** (1997) 361;
L3 Collaboration, M. Acciarri *et al.* , Phys. Lett. **B433** (1998) 163;
L3 Collaboration, M. Acciarri *et al.* , Phys. Lett. **B464** (1999) 135;
L3 Collaboration, M. Acciarri *et al.* , Phys. Lett. **B470** (1999) 281;
L3 Collaboration, M. Acciarri *et al.* , Phys. Lett. **B479** (2000) 101;
L3 Collaboration, M. Acciarri *et al.* , Phys. Lett. **B489** (2000) 81;
OPAL Collaboration, G. Alexander *et al.* , Phys. Lett. **B387** (1996) 432;
OPAL Collaboration, K. Ackerstaff *et al.* , Phys. Lett. **B391** (1997) 221;
OPAL Collaboration, K. Ackerstaff *et al.* , Euro. Phys. J. **C2** (1998) 441;
OPAL Collaboration, G. Abbiendi *et al.* , Euro. Phys. J. **C6** (1999) 1;
OPAL Collaboration, G. Abbiendi *et al.* , Euro. Phys. J. **C13** (2000) 553;

[10] LEP Energy Working Group 99-01;
CERN-EP/98-191

[11] T. Sjöstrand, PYTHIA 5.7/JETSET 7.4 CERN-TH 7112/93 (1993).

[12] F. A. Berends, R. Pittau and R. Kliess, Comp. Phys. Comm. **85** (1995) 437.

[13] S. Nova *et al.* , DELPHI Note 90-35.

[14] F. A. Berends, P. H. Daverveldt and R. Klies, Comp. Phys. Comm. **40** (1986) 271.

[15] S. Jadach, B.F.L. Ward and Z. Was, Comp. Phys. Comm. **79** (1994) 503.

[16] D. Bardin *et al.* , *"ZFITTER: An Analytical Program for Fermion Pair Production in e^+e^- Annihilation"*, HEP-PH/9908433 (1999).

[17] G. Montagna *et al.* , Nucl. Phys. **B401** (1993) 3;
G. Montagna *et al.* , Comput. Phys. Commun. **76** (1993) 328.

[18] E. Eichten, K. Lane and M. Peskin, Phys. Rev. Lett. **50** (1983) 811.

[19] P. Langacker, R.W. Robinett and J.L. Rosner, Phys. Rev. **D30** (1984) 1470;
D. London and J.L. Rosner, Phys. Rev. **D34** (1986) 1530;
J.C. Pati and A. Salam, Phys. Rev. **D10** (1974) 275;
R.N. Mohapatra and J.C. Pati, Phys. Rev. **D11** (1975) 566.

[20] F. James, *"MINUIT Reference Manual"*, CERN Program Library Long Writeup D506 (1994).

[21] A. Leike, Zeit. Phys. **C62** (1994) 265.

[22] G. Altarelli *et al.* , Z. Phys. C45 (1989) 109;
erratum Z. Phys. C47 (1990) 676.

[23] N. Arkani-Hamed *et al.* , Phys. Rev. **D59** (1999) 086004.
J. L. Hewett, Phys. Rev. Lett. **82** (1999) 4765.
G. F. Giudice *et al.* , Nucl. Phys. **B544** (1999) 3.